Phonons in the cubic phase of $Co_3B_7O_{13}X$ (X=Cl, Br, and I) boracites

J. Pascual
Institut Català de Nanotecnologia (ICN) Edifici CM7, Campus de la UAB, 08193 Bellaterra, Barcelona, Spain and Departament de Física Edifici Cn, Universitat Autònoma de Barcelona, 08193 Bellaterra, Barcelona, Spain

Jorge Íñiguez
Institut de Ciencia de Materials de Barcelona (ICMAB-CSIC), Campus UAB, 08193 Bellaterra, Spain

M. N. Iliev, V. G. Hadjiev, and J. Meen
Texas Center for Superconductivity, University of Houston, Texas 77204-5002, USA
(Received 8 December 2008; revised manuscript received 4 February 2009; published 30 March 2009)

The phonon structure in the cubic paraelectric phase ($F\bar{4}3c$) of $Co_3B_7O_{13}X$ (X=Cl,Br,I) boracites has been studied theoretically by density-functional theory and experimentally by Raman spectroscopy. The calculated Raman frequencies are in good agreement with those determined from the polarized Raman spectra. In addition to the four Raman-allowed phonons of A_1 symmetry, a low-frequency broadband of same symmetry is observed in the spectra of $Co_3B_7O_{13}Cl$ and $Co_3B_7O_{13}Br$. The position and width of this band correspond to those of the partial phonon density of states of the halogen vibrations: an indication for disorder and instability of the halogen sublattice. In the case of $Co_3B_7O_{13}I$, an even greater number of spectral features reflecting the underlying phonon density of states are observed. An "instability" F_2 mode that involves displacements of the X atoms along ⟨111⟩ and of the Co atoms along ⟨100⟩ directions is also identified. It is shown that this mode is closely related to the halogen and metal sublattice instabilities, which trigger the cubic to orthorhombic transition at lower temperature.

DOI: 10.1103/PhysRevB.79.104115 PACS number(s): 78.30.−j, 77.84.Bw, 78.20.Bh, 79.60.Ht

I. INTRODUCTION

The increased attention to multiferroicity has revived the interest in the properties of the first discovered multiferroic materials—boracites, $M_3B_7O_{13}X$ (M=divalent metal, X=Cl,Br,I), shortly denoted as M-X. These materials, which are characterized by rich phase diagrams involving various crystallographic and magnetic transitions,[1–6] may present phases in which up to four types of ordering occur simultaneously: ferroelectric, ferroelastic, ferro(ferri)magnetic, and ferrotoroidic (for a review see Ref. 5). The coupling of such orders, already manifested in other multiferroics, is promising for applications, and a lot of efforts are currently dedicated to collecting experimental data and creating theoretical models for the description of the interplay between the magnetic, dielectric, and structural properties. As a part of these efforts, the information on and understanding of lattice dynamics, spin-phonon, and electron-phonon coupling, and the effects of structural and magnetic transitions are of definite importance.

The phonon spectrum of boracites is scarcely studied. To our knowledge, no results on calculations of lattice dynamics of boracites have been reported so far. There are, however, several earlier reports on the polarized Raman spectra of boracites with cubic [Cr-Cl,[7] Ni-I,[8,9] and Cu-Cl (Ref. 10)], orthorhombic [Mn-Cl (Ref. 11)], and trigonal [Zn-Cl (Ref. 12)] structures, as well on the infrared spectra of Ni-I.[13] In the case of cubic boracites, the symmetry of experimentally observed Raman lines has been determined, but no assignment to particular atomic vibrations has been done. It has been assumed[8] that the observed broad low-frequency bands correspond to zone-center Raman-allowed modes, which is unlikely, especially in the case of the A_1 spectra, as by symmetry considerations the A_1 modes involve vibrations of only light boron and oxygen atoms. The symmetry assignment proposed for the Raman lines in the spectra of noncubic boracites has met the problem of coexistence of microtwins with different crystallographic orientation with respect to the incident light polarization.[14,15] The twinning problem has been solved only recently by Raman visualization of twin structure, which makes it possible to measure the spectrum of individual domains with known crystallographic orientation.[16]

As a first step to better understand the phonon structure of boracites, in this work the results of first-principles calculations of the lattice dynamics of cubic Co-I, Co-Br, and Co-Cl are compared with those obtained from the Raman spectroscopy experiments. The good agreement between the predicted and experimentally observed Raman frequencies allowed an assignment of the Raman lines to definite phonon modes. It was found that the additional broadbands in the low-frequency part of the experimental Raman spectra of Co-Cl and Co-Br mirror the calculated partial density of states of halogen vibrations, thus providing evidence for strong disorder of the halogen sublattice. Even more disorder-induced structures were observed in the case of Co-I. One of the Raman modes is found to involve displacements of X atoms along ⟨111⟩ and of Co atoms along ⟨100⟩, which correspond to the orthorhombic distortions in the ferroelectric phase.

II. STRUCTURE AND Γ-POINT PHONONS IN CUBIC BORACITES

The structure of cubic boracites (space group $F\bar{4}3c$, Z=8, No. 219) is illustrated in Fig. 1. The metal and halogen

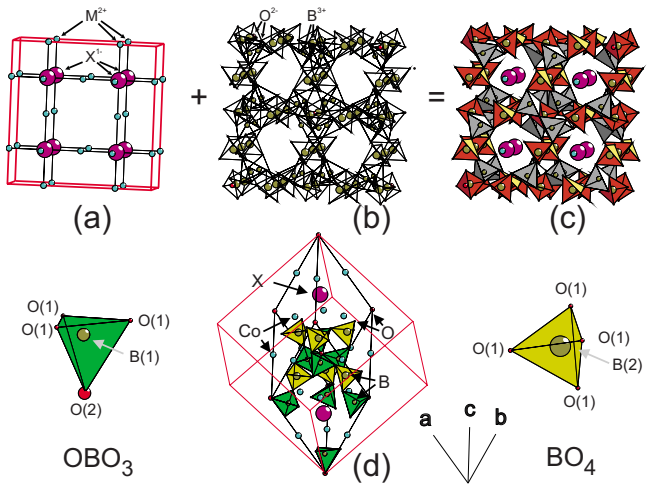

FIG. 1. (Color online) The elementary and primitive cells of cubic *M*-*X* boracite: (a) *M*-*X* sublattice; (b) B-O sublattice; (c) cubic elementary cell (space group $F\bar{4}3c$, $Z=8$, No. 219); and (d) rhombohedral primitive cell ($Z=2$). The two nonequivalent BO_4 and OBO_3 tetrahedral units are also shown. The Raman spectra were collected from the cubic (100) surface.

atoms form a perovskitelike sublattice [Fig. 1(a)], whereas boron and oxygen atoms are connected in a network of two type of corner-sharing BO_4 tetrahedra [Fig. 1(b)]. The rhombohedral primitive cell, which contains 2 formula units (48 atoms) is also shown.

Table I summarizes the results of the group-theoretical analysis for the Γ-point phonons. Of the total of 58 Γ-point phonon modes, 34 ($4A_1+10E+19F_2$) are Raman active, 24 ($6A_2+18F_1$) are silent, and one (F_2) is an acoustic mode. The $19F_2$ modes are also infrared active. Given that the cubic crystallographic directions $X\|[100]$, $Y\|[010]$, $X'\|[110]$, and $Y'\|[1\bar{1}0]$ are known, the symmetry of the Raman lines can be determined experimentally by measuring the polarized Raman spectra with different exact scattering configurations, XX (A_1+E), XY (F_2), $X'X'$ (A_1+E+F_2), and $X'Y'$ (E). The first and second letters in these notations stand for the polarization direction of the incident and scattered lights, respectively. Although there is no polarization configuration where only the A_1 modes are allowed, the pure A_1 spectrum can be obtained by computing the difference between the XX (A_1+E) and $X'Y'$ (E) spectra.

III. LATTICE DYNAMICAL CALCULATIONS, SAMPLES, AND EXPERIMENTAL

For the lattice dynamical calculations, we used the spin-polarized local-density approximation (LSDA) (Ref. 17) to density-functional theory (DFT) as implemented in the VASP code[18] and employed the so-called "LDA+U" correction of Dudarev *et al.*[19] for a better treatment of the Co 3*d* electrons. We used $U=2$ eV, as this was the minimal correction to the LDA that allowed us to obtain, in a computationally robust way, a qualitatively correct description of the magnetic state of the Co ions.[20] We studied in detail the Co-I compound and checked that our quantitative results—as regards the relaxed

TABLE I. Wyckoff notations and irreducible representations for the atoms in the cubic *M*-*X* boracides. The mode classification and the nonzero elements of the Raman tensors are also shown.

Atom	Wyckoff notation	Irreducible representations
M	24*c*	$A_2+E+2F_1+3F_2$
X	8*b*	F_1+F_2
B(1)	32*e*	$A_1+A_2+2E+3F_1+3F_2$
B(2)	24*d*	$A_2+E+2F_1+3F_2$
O(1)	96*h*	$3A_1+3A_2+6E+9F_1+9F_2$
O(2)	8*a*	F_1+F_2

Modes classification

$$\Gamma_{\text{Raman}}=4A_1+10E+19F_2$$
$$\Gamma_{\text{ir}}=19F_2$$
$$\Gamma_{\text{silent}}=6A_2+18F_1$$
$$\Gamma_{\text{acoustic}}=F_2$$

Raman tensors

$$A_1 \rightarrow \begin{bmatrix} a & 0 & 0 \\ 0 & a & 0 \\ 0 & 0 & a \end{bmatrix}$$

$$E \rightarrow \begin{bmatrix} b & 0 & 0 \\ 0 & b & 0 \\ 0 & 0 & -2b \end{bmatrix}, \begin{bmatrix} -\sqrt{3}b & 0 & 0 \\ 0 & \sqrt{3}b & 0 \\ 0 & 0 & 0 \end{bmatrix},$$

$$F_2 \rightarrow \begin{bmatrix} 0 & 0 & 0 \\ 0 & 0 & d \\ 0 & d & 0 \end{bmatrix}, \begin{bmatrix} 0 & 0 & d \\ 0 & 0 & 0 \\ d & 0 & 0 \end{bmatrix}, \begin{bmatrix} 0 & d & 0 \\ d & 0 & 0 \\ 0 & 0 & 0 \end{bmatrix},$$

structure, Co's mangnetic moments, and even phonon spectrum—are not strongly U dependent. In particular, for both $U=2$ eV and $U=4$ eV, we obtained a moment of about $2.6\mu_B$ for the Co ions; unfortunately, as far as we know there are no experimental values to contrast this result.[21] The computed electronic structure shows that the top-valence and bottom-conduction bands have a marked Co 3*d* character, the hybridization with oxygen (and, to a lesser extend, the halogen anions) being significant. We employed the projector augmented wave (PAW) method[22] to represent the ionic cores, solving explicitly for the following electrons: 3*d* and 4*s* of Co, 2*s* and 2*p* of B and O, and the *s* and *p* valence electrons of the halogen atoms (Cl, Br, and I). The electronic wave functions were described with a plane-wave basis truncated at 400 eV, and a $3\times3\times3$ *k*-point grid was used for Brillouin-zone integrations. These calculation conditions were checked to render accurate results. For all Co-*X* compounds, we considered the 48 atom primitive cell of the $F\bar{4}3c$ phase, taking the experimental result for Co-I (Ref. 23) as a starting point for the structural relaxations, which we considered to be converged when residual forces and stresses

were smaller than 10^{-3} eV/Å and 0.01 kbar, respectively.[24] For the *ab initio* relaxed structures, we computed the force-constant matrix associated to the considered unit cell and modeled it in terms of interatomic interactions in real space. This allowed us to then approximate the dynamical matrix at an arbitrary point of the Brillouin zone and thus compute the phonon density of states (PDOS) from a dense grid of k points.[25] Note that all our Co-X boracites are magnetically disordered in their cubic phases. Since modeling magnetic disorder *ab initio* is unfeasible, as one would need to simulate the thermally fluctuating magnetic moments, here we considered a ferromagnetic spin alignment, which has the virtue of not breaking any crystallographic symmetry and is thus a reasonable approximation.

The Raman spectra were collected from as grown (100) cubic surfaces using triple T64000 spectrometer equipped with microscope, heating stage, and liquid nitrogen cooled charge coupled device (CCD) camera. Both 633 nm and 488 nm laser lines have been used for excitation, the spectra being practically the same. As of the three Co-X compounds only Co-I is in its cubic phase at room temperature, the spectra of cubic Co-Br and Co-Cl were measured at 500 and 673 K, respectively, well above the corresponding cubic to orthorhombic transition temperatures of 458 and 623 K.

IV. RESULTS AND DISCUSSION

A. Γ-point Raman phonons

Figure 2 shows the pure A_1, E, and F_2 Raman spectra of cubic Co-X (X=Cl,Br,I) boracites, as extracted from the experimental XX (A_1+E), XY ($E+F_2$), $X'X'$ (A_1+E+F_2), and $X'Y'$ ($E+F_2$) spectra at 673 K for Co-Cl, 500 K for Co-Br, and 295 K for Co-I. The positions of the sharp lines above 200 cm^{-1} in the corresponding spectra of Co-X are very close. This is not unexpected as the phonon frequencies in this range are due to vibrations of light boron and oxygen atoms within the rigid BO_4 and OBO_3 tetrahedra (see Fig. 1), which are practically independent of X. The main difference between Co-Cl and Co-Br spectra is the position of the broad low-frequency band of A_1 symmetry, centered at 162 and 117 cm^{-1}, respectively. The Co-I spectra differ from those of Co-Cl and Co-Br by more complex structure of the low-frequency band (pronounced also in the E and F_2 spectra) and by the presence near 1140 cm^{-1} of a strong structureless wide band, most intense in the E spectrum. Unlike the sharp lines, the broad low- and high-frequency bands do not represent normal Γ-point phonon modes; their origin will be discussed in Sec. IV B.

In Table II are compared the experimental and calculated frequencies of Raman-allowed modes of Co-X. As expected the frequencies of most modes practically do not depend on X. Indeed, by symmetry, mass, and mode mixing considerations, the motions of halogen atoms contribute noticeable only to lowest F_2 modes. The negligible effect of halogen and Co vibrations on the higher-frequency modes is also consistent with the frequency distribution of partial phonon density of states for the nonequivalent atoms in Co-X (see Fig. 3).

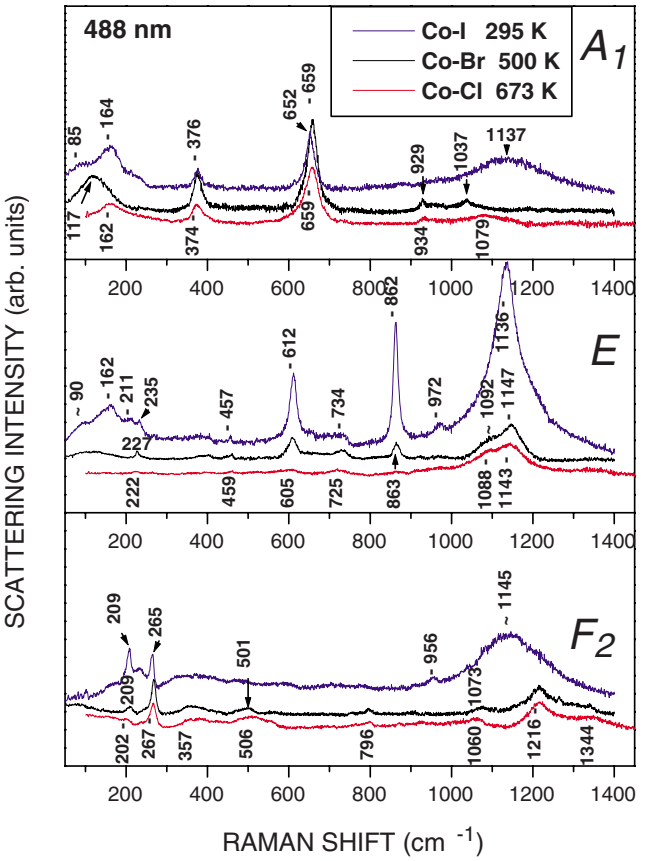

FIG. 2. (Color online) A_1, E, and F_2 Raman spectra of cubic CoI (at 295 K), Co-Br (at 500 K), and Co-Cl (at 673 K) as extracted from the experimental XX A_1+E, XY $E+F_2$, $X'X'$ A_1+E+F_2, and $X'Y'$ $E+F_2$ spectra.

The four A_1 modes involve strongly mixed vibrations of only B(1) and O(1) atoms. The correspondence between the calculated and experimentally observed phonon frequencies for these modes is quite good. The A_1 atomic displacements, as obtained from the DFT calculations for Co-I, are shown in Fig. 4.

In what regards the E and F_2 modes, several points need to be made. First, note that from the calculations we obtained some modes with imaginary frequencies. Such imaginary frequencies imply that the material can reduce its energy if the cubic phase is distorted according to the imaginary-frequency mode eigenvector; they are thus characteristic of crystals undergoing structural phase transitions. Indeed, as we will see below, the F_2 modes with imaginary frequencies are directly related to the ferroelectric phase transitions in our Co-X boracites. Second, a detailed comparison between theory and experiment is difficult for the E and F_2 modes mainly because it was not possible to identify many of these modes from the experimental data. Nevertheless, apart from the uncertainty in the assignment, the correlation between calculated and experimental values for the higher-frequency E and F_2 modes seems quite reasonable.

B. Effects of structural disorder

The broadbands in the spectra of Co-X cannot be assigned to Γ-point Raman modes. This is particularly true for the A_1

TABLE II. Calculated (at 0 K) and experimentally determined frequencies (in cm^{-1}) of the Raman active modes in the cubic phase of Co-I (at 295 K), Co-Br (at 500 K), and Co-Cl (at 673 K).

	Co-I		Co-Br		Co-Cl	
Mode	Theor 0 K	Expt. 295 K	Theor 0 K	Expt. 500 K	Theor 0 K	Expt. 673 K
$A_1(1)$	383	376	383	374	377	374
$A_1(2)$	678	652	669	659	639	659
$A_1(3)$	897		894	929	899	934
$A_1(4)$	1077		1080	1037	1087	1079
$E(1)$	63		*i*27		*i*65	
$E(2)$	226	230	240	227	232	222
$E(3)$	414		420	405	413	
$E(4)$	452	457	460	458	456	459
$E(5)$	625	612	628	608	633	605
$E(6)$	759	734	758	734	767	725
$E(7)$	860	862	883	863	886	868
$E(8)$	1036	972	1049	1092	1051	1088
$E(9)$	1153		1189	1142	1177	1143
$E(10)$	1235		1252		1254	
$F_2(1)$	*i*79		*i*60		*i*122	
$F_2(2)$	≈0	acoust	≈0	acoust	≈0	acoust
$F_2(3)$	92		99		176	
$F_2(4)$	187	209	196	209	186	202
$F_2(5)$	221		234		238	
$F_2(6)$	257	265	268	267	281	267
$F_2(7)$	353		352	355	349	
$F_2(8)$	382		388		393	
$F_2(9)$	431		466		474	
$F_2(10)$	543		529	501	539	506
$F_2(11)$	585		591		599	
$F_2(12)$	610		615		615	
$F_2(13)$	676		679		682	
$F_2(14)$	800		805	796	808	796
$F_2(15)$	887		896		904	
$F_2(16)$	1005	956	1016		1024	
$F_2(17)$	1020		1027		1036	
$F_2(18)$	1082		1094	1079	1102	1060
$F_2(19)$	1111		1134		1143	
$F_2(20)$	1191		1204	1216	1210	1216

spectra, where no phonons are expected below 300 cm^{-1}. The frequency ratio of the low-energy A_1 bands of Co-Cl and Co-Br, $\omega_{\text{Co-Cl}}/\omega_{\text{Co-Br}}=162/117=1.38$, roughly scales with halogen mass ratio $(m_{\text{Br}}/m_{\text{Cl}})^{1/2}=1.50$. Such correlation is a strong indication that the bands are related to vibrations involving mainly displacements of halogen atoms. A reasonable explanation for observation of these, otherwise Raman forbidden vibrations, could be a disorder of the halogen sublattice.

The loss of translational symmetry in this case should result in the breaking of the momentum conservation law and

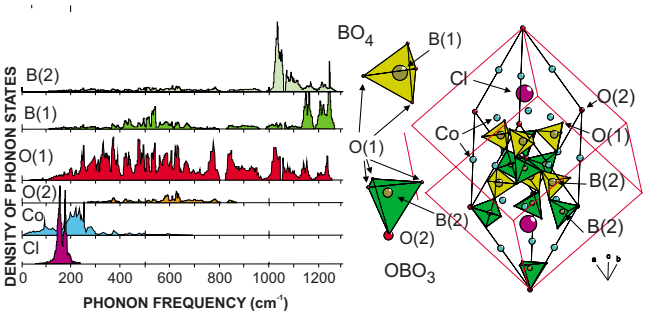

FIG. 3. (Color online) Partial phonon density of states related to vibrations of the nonequivalent atoms Co, B(1), B(2), O(1), O(2), and Cl in the cubic phase of Co-Cl. (Detailed information on the computed interatomic force constants is available from the authors upon request.)

the activation in the Raman spectra of all out-of-center phonon states of the corresponding phonon branches. The spectral profile of disorder-activated scattering should roughly represent the smeared partial density of states (PDOS) of halogen vibrations in the ordered material. Under "smeared PDOS" one understands PDOS where the delta functions $\delta(\omega_{\text{ph}}-\omega)$, used to characterize the frequency of individual phonons in an ideal crystal, are replaced by normalized Lorentzian functions $L(\omega)=\frac{1}{\pi}\frac{\gamma}{(\omega-\omega_{\text{ph}})^2+\gamma^2}$, where γ is the Lorentzian's half width, determined by the finite phonon lifetime $\tau=1/\gamma$. That such density of states might be at the origin of the broad low-frequency A_1 bands in Co-Cl and Co-Br is strongly supported by the fact that, as seen in Fig. 5, the band position and width are in excellent agreement with those of the partial PDOS for the Cl and Br vibrations.

The interpretation of the low-energy part of the spectra in terms of disordered-activated Raman scattering is consistent with other experimental data on cubic boracites.[26–28] Single crystal x-ray data for the cubic phase of Mg-Cl have indicated that the Cl and Mg atoms are disordered within ordered

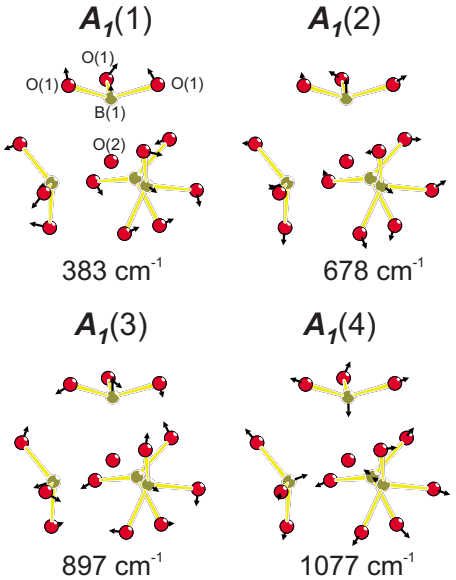

FIG. 4. (Color online) Atomic displacements of the A_1 modes as obtained from the DFT calculation for Co-I.

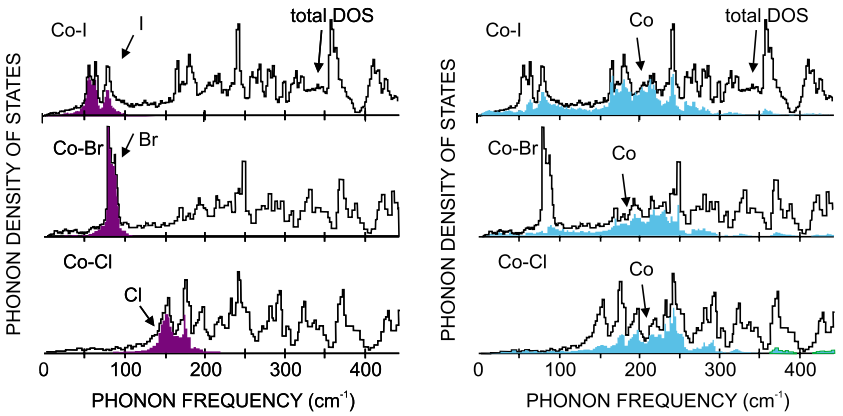

FIG. 5. (Color online) Total and partial phonon density of states related to halogen (I,Br, and Cl) and cobalt vibrations as obtained from the DFT calculation for Co-I, Co-Br, and Co-Cl.

borate framework.[26] X-ray diffuse scattering experiments on Ni-I, Fe-Br, Cu-Cl, and Cr-Cl have shown that in the cubic phase there are correlated displacements of halogen atoms along the ⟨111⟩ and metal atoms along the ⟨100⟩ directions.[27] The temperature-dependent extended x-ray-absorption fine structure (EXAFS) study through the orthorhombic to cubic transition of Fe-Br has provided clear evidence that Br-Fe atomic distribution in the cubic phase is similar to that in the low-temperature ferroelectric phase, which indicates that the cubic phase is essentially disordered.[28]

Given that the halogen (Cl, Br or I) sublattice is disordered, the natural question is to what extent the rest of the structure is also affected and whether this is reflected in the Raman spectra. The answer could be given accounting for the interatomic distances in cubic boracites.[23,29–32] As it follows from the structural data, the *X*-*M* distance between a halogen atom and its nearest neighbors *M* is ≈3.0 Å, is much larger than *M*-O(1)(≈2.1 Å), B(1)-O(1)(≈1.4 Å), and B(1)-O(2)(≈1.7 Å) distances. It is, therefore, reasonable to expect that only relatively strong displacements of halogen atoms from their positions in the ideal sublattice will have noticeable effect on the neighboring metal atoms and indirectly on the next-nearest neighbors, the O(1) atoms. It seems the latter is exactly what takes the place in Co-I. The low-frequency band in this case has a complex profile and its frequency range covers those of both I and Co partial PDOSs (see Figs. 2 and 5). Moreover, a rather strong broadband centered at ≈1140 cm^{-1} is pronounced in the Co-I spectra. This band differs significantly from the spectral structures of Co-Cl and Co-Br in the same frequency range and can hardly be assigned to a single phonon or few overlapping phonon lines. The most plausible explanation for these additional broad spectral features is stronger disorder of Co-I structure, which spreads not only over I, but also Co, and O(1) sites.

C. Instability modes

As already mentioned, the imaginary values of the $E(1)$ and $F_2(1)$ phonon frequencies obtained from the DFT calculations are indicative of structural instabilities. It is therefore of definite interest to verify whether the displacements involved in these computationally unstable modes are related to the lattice distortions in the ferroelectric orthorhombic phase.

Figure 6 shows a component of the triply degenerate $F_2(1)$ mode as obtained from the DFT calculations. Only *X* and *M* atoms are shown as the displacements of B and O are negligibly small. The vibrations of the *X* atoms in the $F_2(1)$ mode are along the ⟨111⟩ diagonals of the cubic elementary cell, whereas those of *M* atoms are along the cubic ⟨100⟩ direction. These are exactly the displacements known to freeze in the orthorhombic phase and to produce the ferroelectric state.[33] Therefore the $F_2(1)$ mode is closely associated with the dominant structural instability, and we call it here the instability mode. Unfortunately, the $F_2(1)$ mode has not been experimentally identified yet. More detailed studies of the Raman spectra modification across the cubic-to-orthorhombic phase transition are needed to clarify whether this mode is an order-parameter soft mode that drives the transition or it is simply a mode compatible with the cubic phase structural instability. As regards the unstable modes with *E* symmetry, they represent *weaker* instabilities of the cubic phase (as already suggested by the relatively small magnitude of their imaginary frequencies) that could either (i) become stable once the material transits to its ferroelectric phase or (ii) lead to structural phase transitions at lower temperatures. Investigating such possibilities falls beyond the scope of the present study.

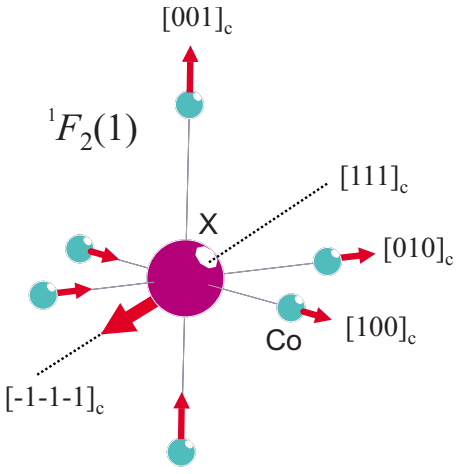

FIG. 6. (Color online) Atomic displacements of the triply degenerate $F_2(1)$ mode. The boron and oxygen atoms are not shown as their motions do not contribute significantly to this mode.

V. CONCLUSIONS

The combined experimental and theoretical studies of the phonons in the cubic phase of Co-X (X=Cl,Br,I) boracites allowed a reliable assignment of all features in the Raman spectra to definite Γ-point phonons or disorder-induced scattering reflecting the density of states of selected phonon branches. Given that the disorder scattering, related to X and to some extent M, has been observed in all Raman studies of cubic boracites, we conclude that the disorder over the halogen sublattice is inherent for the cubic boracites. We also identify computationally an instability F_2 mode that involves exclusively motions of X and M atoms and atomic displacements mimicking the orthorhombic distortions of the ferroelectric phase.

ACKNOWLEDGMENTS

We thank M. E. Mendoza, J. P. Rivera, and H. Schmid for providing the samples used in the experiments. The discussions with H. Schmid are highly appreciated. This work was supported in part by the State of Texas through the Texas Center for Superconductivity at the University of Houston under Grant No. TK-X-1712/2007 of the Bulgarian Science Fund, as well as by the Spanish (Grants No. FIS2006-12117-C04-01 and No. CSD2007-00041) and Catalan (Grant No. SGR2005-683) Governments.

[1] R. J. Nelmes, J. Phys. C **7**, 3840 (1974).
[2] P. Toledano, H. Schmid, M. Clin, and J. P. Rivera, Phys. Rev. B **32**, 6006 (1985).
[3] H. Schmid, H. Rieder, and E. Ascher, Solid State Commun. **3**, 327 (1965).
[4] G. Quézel and H. Schmid, Solid State Commun. **6**, 447 (1968).
[5] H. Schmid, J. Phys.: Condens. Matter **20**, 434201 (2008).
[6] W. Schnelle, E. Gmelin, and H. Schmid, (unpublished).
[7] D. J. Lockwood, Solid State Commun. **18**, 115 (1976).
[8] A. F. Murray and D. J. Lockwood, J. Phys. C **11**, 2349 (1978).
[9] A. F. Murray and D. J. Lockwood, J. Phys. C **11**, 4651 (1978).
[10] D. J. Lockwood and R. W. G. Sime, Ferroelectrics **21**, 557 (1978).
[11] D. J. Lockwood, Indian J. Pure Appl. Phys. **16**, 268 (1978).
[12] D. J. Lockwood, Ferroelectrics **29**, 19 (1980).
[13] J. Petzelt and I. Mayerová, Czech. J. Phys., Sect. B **23**, 1277 (1973).
[14] H. Schmid, Phys. Status Solidi **37**, 209 (1970).
[15] M. N. Iliev, V. G. Hadjiev, J. Íñiguez, and J. Pascual, Acta Physica. Pol. (to be published).
[16] M. N. Iliev, V. G. Hadjiev, M. E. Mendoza, and J. Pascual, Phys. Rev. B **76**, 214112 (2007).
[17] J. P. Perdew and A. Zunger, Phys. Rev. B **23**, 5048 (1981); D. M. Ceperley and B. J. Alder, Phys. Rev. Lett. **45**, 566 (1980).
[18] G. Kresse and J. Furthmuller, Phys. Rev. B **54**, 11169 (1996).
[19] S. L. Dudarev, G. A. Botton, S. Y. Savrasov, C. J. Humphreys, and A. P. Sutton, Phys. Rev. B **57**, 1505 (1998).
[20] For U=0 we often obtained a qualitatively wrong solution without localized magnetic moments, as well as a unphysically strong sensitivity of the electronic solution to small structural distortions.
[21] As discussed in Ref. 3, for many boracites the experimentally determined magnetic moments are higher than the spin-only values, which suggest a strong orbital contribution and preclude comparison with our theory.
[22] P. E. Blochl, Phys. Rev. B **50**, 17953 (1994); G. Kresse and D. Joubert, *ibid.* **59**, 1758 (1999).
[23] R. J. Nelmes and W. J. Hay, J. Phys. C **14**, 5247 (1981).
[24] In the structural relaxations, only the cell volume V_{conv} and positions of the B(1) [Wyckoff orbit 32e, representative atom at (x,x,x)] and O(1) [Wyckoff orbit 96h, representative atom at (x',y',z')] atoms need to be determined. Our results are the following. For Co-Cl: V_{conv}=1632 Å^3, x=0.0799, x'=0.1800, y'=0.0168, and z'=0.0994. For Co-Br: V_{conv}=1649 Å^3, x=0.0800, x'=0.1800, y'=0.0172, and z'=0.0992. For Co-I: V_{conv}=1655 Å^3, x=0.0796, x'=0.1796, y'=0.0168, and z'=0.0988. In the case of Co-I, our results (with correspond to the 0 K limit) are in reasonable agreement with the room-temperature data of Nelmes *et al.*,[23] who obtained V_{conv}=1780 Å, x=0.0797, x'=0.1803, y'=0.0196, and z'=0.0966.
[25] We did not calculate the LO-TO splittings associated to the F_2 modes, something that would have been very computationally costly. Thus, all our computed frequencies correspond to transversal modes, which seemed sufficient for this study. Indeed, as it was shown experimentally for the case of Co-Cl,[16] the LO-TO splittings are very small.
[26] S. Sueno, J. R. Clark, J. J. Papike, and J. A. Konnert, Am. Mineral. **58**, 691 (1973).
[27] P. Felix, M. Lambert, R. Comes, and H. Schmid, Ferroelectrics **7**, 131 (1974).
[28] T. I. Nedoseykina, V. A. Shuvaeva, I. V. Pirog, A. T. Shuvaev, K. Yagi, Y. Azuma, and H. Terauchi, Ferroelectrics **284**, 175 (2003).
[29] A. Monnier, G. Berset, H. Schmid, and K. Yvon, Acta Crystallogr., Sect. C: Cryst. Struct. Commun. **43**, 1243 (1987).
[30] R. J. Nelmes and F. R. Thorney, J. Phys. C **9**, 665 (1976).
[31] G. Berset, W. Depmeier, R. Boutellier, and H. Schmid, Acta Crystallogr., Sect. C: Cryst. Struct. Commun. **41**, 1694 (1985).
[32] O. Crottaz, F. Kubel, and H. Schmid, J. Solid State Chem. **120**, 60 (1995).
[33] J.-P. Rivera, Ferroelectrics **21**, 455 (1978).